Available online at www.sciencedirect.com
SCIENCE DIRECT®
Advances in Space Research 34 (2004) 700–709
ADVANCES IN SPACE RESEARCH (a COSPAR publication)
www.elsevier.com/locate/asr

The Orbiting Carbon Observatory (OCO) mission

D. Crisp [a,*], R.M. Atlas [b], F.-M. Breon [c], L.R. Brown [a], J.P. Burrows [d], P. Ciais [c], B.J. Connor [e], S.C. Doney [f], I.Y. Fung [g], D.J. Jacob [h], C.E. Miller [i], D. O'Brien [j], S. Pawson [b], J.T. Randerson [k,l], P. Rayner [j], R.J. Salawitch [a], S.P. Sander [a], B. Sen [a], G.L. Stephens [m], P.P. Tans [n], G.C. Toon [a], P.O. Wennberg [k,l], S.C. Wofsy [h], Y.L. Yung [k], Z. Kuang [k], B. Chudasama [a], G. Sprague [a], B. Weiss [a], R. Pollock [o], D. Kenyon [p], S. Schroll [p]

[a] *Jet Propulsion Laboratory, California Institute of Technology, 4800 Oak Grove Drive, Pasadena, CA 91109, USA*
[b] *NASA Goddard Space Flight Center, Mail Code 910.3, Greenbelt, MD 20771, USA*
[c] *Laboratoire des Sciences du Climat et de l' Environment UMR 1572, Bat 709, CE L'Orme des Merisies, 1191 Gif sur Yvettee, France*
[d] *Institut für Umweltphysik/Institut für Fernerkundung, Fachberich 1, Universität Bremen,Postfach 330440, 28334 Bremen, Germany*
[e] *National Institute of Water and Atmospheric Research PB 50061, Omakau 9182, New Zealand*
[f] *Marine Chemistry and Geochemistry Department, Woods Hole Oceanographic Institution, Woods Hole, MA 02543, USA*
[g] *Berkeley Atmospheric Sciences Center, University of California, Berkeley, CA 94720-4767, USA*
[h] *Pierce Hall, 29 Oxford St., Harvard University, Cambridge, MA 02138, USA*
[i] *Department of Chemistry, Haverford College, 370 Landcaster Ave., Haverford, PA 19041-1392, USA*
[j] *CSIRO Atmospheric Research, Aspendale, Vic. 3195, Australia*
[k] *Division of Geological and Planetary Sciences, California Institute of Technology, Pasadena, CA 91125, USA*
[l] *Division of Engineering and Applied Sciences, California Institute of Technology, Pasadena, CA 91125, USA*
[m] *Colorado State University Department of Atmospheric Science, FortCollins, CO 80523-1371, USA*
[n] *Climate Monitoring & Diagnostics Laboratory, 325 Broadway R/CMDL, Boulder, CO 80305, USA*
[o] *Hamilton Sundstrand Sensor Systems, 2771 North GareyAve., Pomona, CA 91767, USA*
[p] *Orbital Sciences Corporation, 21839 Atlantic Blvd., Dulles, VA 20166, USA*

Received 19 October 2002; received in revised form 5 April 2003; accepted 5 August 2003

Abstract

The Orbiting Carbon Observatory (OCO) mission will make the first global, space-based measurements of atmospheric carbon dioxide (CO_2) with the precision, resolution, and coverage needed to characterize CO_2 sources and sinks on regional scales. The measurement approach and instrument specifications were determined through an analysis of existing carbon cycle data and a series of observing system simulation experiments. During its 2-year mission, OCO will fly in a 1:15 PM sun-synchronous orbit with a 16-day ground-track repeat time, just ahead of the EOS Aqua platform. It will carry a single instrument that incorporates three bore-sighted high-resolution spectrometers designed to measure reflected sunlight in the 0.76-μm O_2 A-band and in the CO_2 bands at 1.61 and 2.06 μm. Soundings recorded in these three bands will be used to retrieve the column-averaged CO_2 dry air mole fraction (X_{CO_2}). A comprehensive validation program was included in the mission to ensure that the space-based X_{CO_2} measurements have precisions of ~0.3% (1 ppm) on regional scales. OCO measurements will be used in global synthesis inversion and data assimilation models to quantify CO_2 sources and sinks. While OCO will have a nominal lifetime of only 2 years, it will serve as a pathfinder for future long-term CO_2 monitoring missions.

Keywords: Orbiting carbon observatory; Atmospheric carbon dioxide

* Corresponding author. Tel.: +1-818-354-2224; fax: +1-818-393-0071.
E-mail address: david.crisp@jpl.nasa.gov (D. Crisp).

0273-1177/$30 © 2004 COSPAR. Published by Elsevier Ltd. All rights reserved.
doi:10.1016/j.asr.2003.08.062

1. Introduction

Carbon dioxide (CO_2) is an efficient greenhouse gas, whose atmospheric concentration has increased from 280 to 370 parts per million (ppm) since the beginning of the industrial age (Fig. 1(a); Cicerone et al., 2001). These rapid increases have raised concerns about global climate change. For more than 20 years, data collected from a global network of surface stations indicate only about half of the CO_2 that has been emitted into the atmosphere by fossil fuel combustion and biomass burning has remained there (Fig. 1(b); cf. Schnell et al., 2001; Etheridge et al., 1996). The terrestrial biosphere and oceans have apparently absorbed the rest. The nature and geographic distribution of these CO_2 sinks is not well understood. Specifically, while data from the Globalview-CO_2 database (GV-CO2; cf. Gloor et al., 2000) provide compelling evidence for a Northern Hemisphere terrestrial carbon sink, this network is too sparse to resolve North American and Eurasian contributions to this sink, or to estimate fluxes over the southern oceans (Battle et al., 2000; Bousquet et al., 2000; Ciais et al., 1995; Conway and Tans, 1999; Denning et al., 1995; Keeling and Shertz, 1992; Morimoto et al., 2000; Pacala et al., 2001; Tans et al., 1989; Fan et al., 1998; Rayner and O'Brien, 2001; Enting, 1993). Existing measurements and models also cannot fully explain why the atmospheric CO_2 increase has varied from 1 to 7 gigatons of carbon (GtC) per year in response to steadily rising fossil fuel emission rates (Fig. 1(b); Randerson et al., 1997, 1999; Lee et al., 1998; Le Quéré et al., 2000; Keeling et al., 1995; Houghton, 2000; Frolking et al., 1996; Langenfelds et al., 2002). Because the present-day behavior of these CO_2 sinks is not understood, predictions of their response to future climate or land use changes have large uncertainties. If their efficiency decreases over time, the atmospheric CO_2 buildup could accelerate (Cox et al., 2000; Friedlingstein et al., 2001).

Global simulations with source–sink synthesis inversion models (Rayner and O'Brien, 2001) indicate that uncertainties in the atmospheric CO_2 balance could be reduced substantially if data from the existing ground-based CO_2 network were augmented by spatially resolved, global, measurements of the column-integrated dry air mole fraction (X_{CO_2}) with precisions of ~1 ppm (0.3% of 370 ppm). This information would also facilitate monitoring compliance with future CO_2 emissions treaties that offer credits for CO_2 sequestration as well as emissions reductions. The Orbiting Carbon Observatory (OCO) has been designed to provide these measurements.

2. Measurement approach

Synthesis inversion models infer the flux of CO_2 between the surface and atmosphere from measured spatial and temporal gradients in the atmospheric CO_2 concentration. Because these gradients are usually small (<1 ppm) on regional scales ($8° \times 10°$), X_{CO_2} measurements must have high precision and no significant geographically varying bias at regional to continental scales. To meet these stringent requirements, the OCO measurement requirements were derived from end-to-end observation system simulation experiments. A spectrum resolving (line-byline), multi-stream, multiple scattering model (cf. Crisp, 1997) was used to generate realistic, spectrally resolved radiances for a broad range of solar zenith angles and combinations of atmospheric and surface properties (cloud, aerosol, temperature, humidity, CO_2 profiles, surface pressures and surface albedos). These synthetic spectra were processed with an instrument simulation model that specified the spatial resolution, spectral range and resolving power, instrument line shape, optical throughput, detector quantum efficiency and linearity, scattered light, as well as other known noise sources. Estimates of X_{CO_2} were then derived with a remote sensing retrieval algorithm based on optimal estimation retrieval theory (Rodgers, 1976; Rodgers, 2000; Kuang et al., 2002). Results from these X_{CO_2} retrieval experiments were combined with constraints derived from carbon cycle models to define the instrument spectral range, resolving power, spatial coverage and resolution, signal-to-noise ratio, and validation strategy.

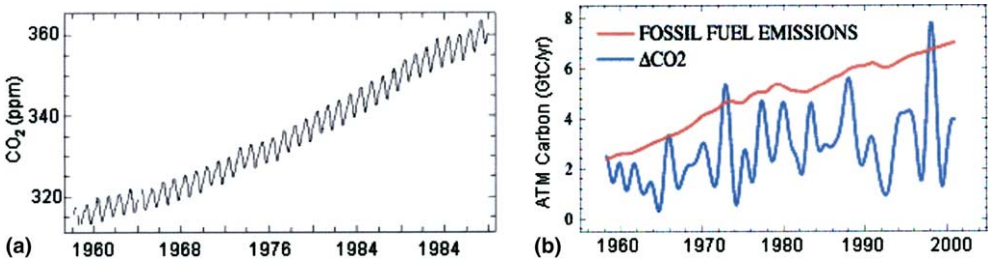

Fig. 1. (a) A 40-year history of atmospheric CO_2. (b) Observed variations in annual atmospheric CO_2 accumulation (ΔCO_2) compared with fossil fuel emissions (cf. Schnell et al., 2001; Houghton et al., 2001). Significant changes in carbon sequestration occur from year to year in the presence of uniform increases in fossil fuel emissions.

2.1. Spectral range

High-resolution spectroscopic observations of near infrared (IR) CO_2 absorption bands in reflected sunlight were selected for this application because they provide high sensitivity near the surface, where most CO_2 sources and sinks are located. In contrast, thermal IR techniques have less sensitivity near the surface because the thermal contrast between the surface and near surface atmosphere is often small (Fig. 2).

Several factors besides the atmospheric CO_2 mole fraction contribute to the CO_2 absorption intensity measured from space. These factors include the solar zenith angle, surface pressure, the atmospheric temperature and humidity profiles, and the instrument pointing geometry. Clouds, aerosols, and surface topography further complicate efforts to retrieve the CO_2 mole fractions from space-based CO_2 absorption measurements because they introduce additional uncertainties in the atmospheric optical path length. Accurate measurements of the CO_2 absorption are therefore necessary, but not sufficient, to infer surface–atmosphere carbon fluxes from space-based measurements. While environmental variables such *as* surface pressure, atmospheric temperature, and humidity are adequately constrained on regional scales, these properties are generally not known at the much smaller spatial scales needed to resolve clouds or surface topography variations. These systematic errors can be minimized by deriving X_{CO_2} from simultaneous CO_2 and O_2 soundings: $X_{CO_2} = [O_2](\text{column } CO_2)/(\text{column } O_2)$, where $[O_2] = 0.2095$ is the O_2 mole fraction. OCO will retrieve X_{CO_2} from high-resolution spectroscopic measurements of reflected sunlight in the CO_2 bands at wavelengths near 1.61 and 2.06 microns (μm), and the O_2 A-band at 0.76 μm. Simultaneous, bore-sighted observations from these three bands constitute a *single sounding*. Each sounding will be analyzed with an algorithm that incorporates an atmospheric radiative transfer model, an instrument simulator model, and a retrieval algorithm that adjusts the assumed atmospheric state to better match the measurements.

The weak CO_2 band near 1.61 μm was selected as the primary candidate for CO_2 column measurements for three reasons. First, this spectral region is relatively free of absorption by other gases. Second, few of the spectral lines in this band saturates for the range of observing conditions considered here, so that their absorption increases almost linearly with the CO_2 abundance and path length. Third, thermal emission from the atmosphere and instrument are negligible at these wavelengths, simplifying the instrument design and radiometric calibration.

Measurements of a reference gas whose concentration is uniform, constant and well known are also needed to derive X_{CO_2} from space-based measurements of the CO_2 absorption. Molecular oxygen is the best available candidate. OCO will use bore-sighted, high spectral resolution O_2 A-band (0.76 μm) observations for this purpose. Aircraft studies show that A-band observations can provide surface pressure estimates with accuracies of ~1 mbar (0.1%; O'Brien and Mitchell, 1992), exceeding the OCO 0.3% X_{CO_2} accuracy requirement. Clouds and aerosols can absorb or scatter sunlight back to space before it traverses the entire atmospheric column, precluding full-column CO_2 measurements. The O_2 A-band is equally sensitive to clouds and more sensitive to small aerosol particles than the 1.61-μm CO_2 band (O'Brien and Mitchell, 1992; Heidinger and Stephens, 2000). O_2 A-band measurements will therefore be used to characterize the vertical distribution of clouds and aerosols in each sounding. Those soundings with a scattering optical depth is $\tau_s > 0.3$ will be rejected.

For less opaque soundings ($\tau_s < 0.3$), cloud and aerosol scattering can introduce errors in the retrieved X_{CO_2} by adding uncertainty to the photon path length. O_2 A-band observations can constrain the distribution and optical properties of liquid water clouds, but these observations are not adequate to characterize the scattering by water ice clouds and aerosols at longer near-IR wavelengths because the optical properties of these airborne particles vary with wavelength. Our retrieval experiments show that the effects of ice clouds and aerosols can be characterized by combining simulta-

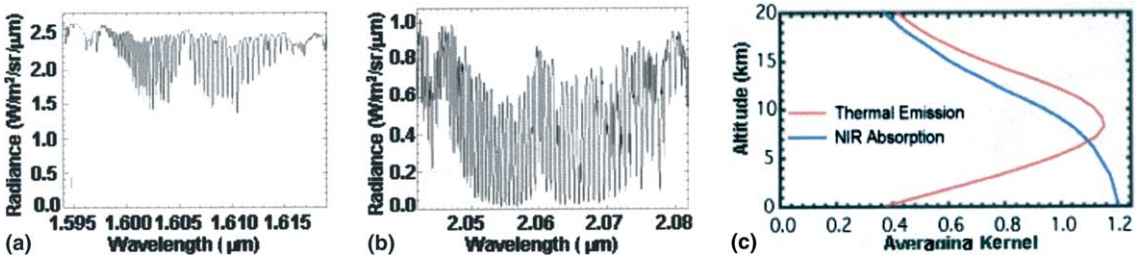

Fig. 2. (a), (b) Simulated radiances over a moderately dark ocean surface in the 1.61- and 2.06-μm CO_2 bands at a solar zenith angle of 60°. (c) Representative vertical averaging kernels for column CO_2 soundings using near IR absorption of reflected sunlight in the 1.61-μm CO_2 band (blue) and thermal IR emission near 14.3 μm (red). Thermal IR soundings are less sensitive to near-surface CO_2 because of the small surface–atmosphere temperature contrast.

neous spectroscopic observations from the O_2 A-band and the CO_2 bands near 1.61 and 2.06 μm. These two bands provide independent constraints on CO_2 and aerosols because the strongly saturated lines in the 2.06-μm CO_2 band have a weaker dependence on the CO_2 concentration and greater sensitivity to airborne particles than the weak lines in the 1.61-μm band.

In the baseline design, the spectral range for each channel includes the complete molecular absorption band as well as some continuum at both ends. This full-band approach minimizes biases due to uncertainties in atmospheric temperature, which affect the relative strengths of individual rotational transitions. The continuum at the band edges provides constraints on the wavelength dependent optical properties of the surface albedo and airborne particles.

2.2. Spectral resolving power

Our simulations showed that high spectral resolution is required to maximize sensitivity and minimize systematic measurement errors. A spectral resolving power, $R = \lambda/\Delta\lambda \sim 21,000$ separates individual CO_2 lines in the 1.61-μm region from weak H_2O and CH_4 lines and from the underlying continuum (Fig. 2). Higher resolving powers can yield greater sensitivity, but they give an unacceptably low signal-to-noise ratio (SNR) for the instrument architecture and spatial sampling scales adopted for OCO. For the O_2 A-band, a resolving power of $R \sim 17{,}500$ is needed to distinguish the O_2 doublets from the continuum. With these resolving powers, the OCO retrieval algorithm can characterize the surface albedo throughout the band and solve for the wavelength dependence of the aerosol scattering, minimizing X_{CO_2} retrieval errors contributed by uncertainties in the continuum level.

2.3. Orbit requirements

Because CO_2 concentrations near the surface vary over the diurnal cycle, orbits with both fixed and processing equator crossing times were considered for OCO. Measurements acquired from a processing orbit would provide some information about the CO_2 diurnal cycle, but it would be impossible to discriminate diurnal effects from east-west gradients in X_{CO_2}. A fixed equator crossing time samples all regions of the Earth at the same local time of day. Although this orbit provides no constraint on the diurnal cycle, it yields identical Sun–Earth–satellite observing geometry along any given latitude circle, minimizing confusion between spatial and temporal X_{CO_2} variations. It therefore minimizes the east–west biases along a given latitude circle contributed by variations in viewing geometry. This approach was adopted for OCO to help ensure the accuracy of the small, east–west X_{CO_2} gradients. An equator crossing time near noon was selected because: (i) the Sun is high in the sky, maximizing the signal to noise of the X_{CO_2} measurements, (ii) in situ data show CO_2 concentrations over land are often near their diurnally averaged values at that time, and (iii) the planetary boundary layer is deep and slowly varying, facilitating efforts to validate the space-based CO_2 observations with ground-based, flux tower, and aircraft measurements.

OCO will fly in a sun-synchronous, 705 km altitude orbit with a 1:15 PM equator crossing time. It will fly 15 min ahead of the EOS Aqua platform, sharing its ground track and that of other spacecraft in the Earth Observing System (EOS) Afternoon Constellation (A-Train). This orbit facilitates comparisons of OCO observations with complementary data taken by Aqua, Aura, and other A-Train missions (CloudSat, CALIPSO and PARASOL). This orbit's 16-day repeal cycle also facilitates monitoring X_{CO_2} variations on semi-monthly time scales.

2.4. Science observing modes

OCO will use three science observation modes. In Nadir mode, the satellite will point the instrument at the local nadir to collect data along the ground track. This mode provides the highest spatial resolution, but may not provide adequate signal to noise over dark ocean surfaces. In Glint mode, the spacecraft will point the instrument toward the bright "glint" spot, where solar radiation is specularly reflected from the surface. Glint measurements will provide much higher SNR over the ocean. OCO will switch from Nadir to Glint modes on alternate 16-day global ground-track repeat cycles. Finally, Target mode will be used to track specific surface targets as the satellite flies overhead. This mode will provide up to 24,000 samples over sites that include ground-based calibration assets.

2.5. Spatial sampling

The OCO spatial sampling requirements were derived from two considerations. First, while many soundings must be collected to adequately sample the CO_2 abundance on regional scales, contiguous spatial sampling is not required because the atmosphere transports CO_2 over a large area as it is mixed throughout the column. Second, the full atmospheric column must be sampled to provide useful constraints on surface CO_2 sources and sinks. A small footprint will minimize the effects of clouds, which preclude full-column CO_2 measurements.

To address these issues, each OCO spectrometer will have a 10-km wide field of view (FOV) at nadir that is divided into 10, 1-km wide samples (Fig. 3(b)). Spectral soundings are collected at a rate of 4.5 Hz as the spacecraft moves along its ground track at 6.78 km/s,

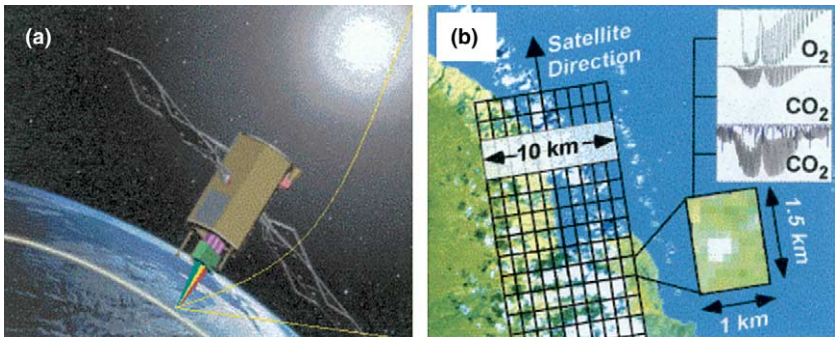

Fig. 3. (a) OCO spacecraft orbiting the Earth in Nadir Sounding mode, (b) Landsat image of Hilo Bay, Hawaii illustrating the OCO spatial sampling approach. Ten 1-km wide cross-track samples are collected in each of the three wavelengths at 4.5 Hz along the orbit track. At nadir this yields a footprint with dimensions of 1 km × 1.5 km.

yielding a 1.5 km down-track resolution at nadir. This yields ~740 soundings per degree of latitude along the orbit track. The footprint size can vary in glint and target modes, but will not exceed 10 km^2 even at large spacecraft nadir angles (~60°). This sampling approach will yield adequate constraints on X_{CO_2} even in regions occupied by patchy clouds (Rayner et al., 2002).

2.6. End-to-end retrieval tests

Fig. 4 shows results from the end-to-end tests of the retrieval algorithm. In these tests, atmospheric and surface properties were varied randomly over the full range of expected values, with sub-visual cirrus and thin to moderate aerosols, for solar zenith angles (SZA) of 35° and 75°. Nadir soundings over both an ocean surface (albedo, $a(0.76\mu m) \sim 0.06$) and brighter desert surfaces ($a(0.76\ \mu m) \sim 0.2$) are shown. Simultaneous retrievals from the three bore-sighted spectral channels yielded X_{CO_2} retrievals with standard deviations of 0.2–0.5% (0.8–1.7 ppm X_{CO_2}. The errors grow to ~6 ppm if the 2.06-μm channel is eliminated. The largest errors occur for hazy conditions over dark surfaces at high SZA. Observations of bright surfaces or Sun glint over the oceans yield smaller errors (Kuang et al., 2002). Fig. 4(b) shows how errors decrease with the number of soundings. Simulations with all three spectral channels (red) reach the accuracy target (1 ppm) quickly, even in partially cloudy regions.

2.7. Correlative measurement requirements

The OCO calibration and validation (Cal/Val) effort is based on the TOMS model, which succeeded in producing global maps of changes in atmospheric ozone with a relative accuracy of better than 1%. For OCO, both in situ and remote sensing measurements will be used to validate the X_{CO_2} retrievals. The core of the surface CO_2 measurement program will consist of the existing NOAA Climate Monitoring and Diagnostics Laboratory (CMDL) network of flask stations (Conway et al., 1994). A few stations will be upgraded to provide continuous measurements throughout the diurnal cycle. These flask data will be augmented by pCO_2 measurements from moorings (e.g. the Tropical Atmosphere-Ocean and Pirana buoy arrays) and in situ non-dispersive IR data from the FLUXNET towers (Baldocchi et al., 2001). These in situ data will constrain the near-surface CO_2 concentrations and help to quantify the diurnal, seasonal, and clear-sky biases in the satellite data.

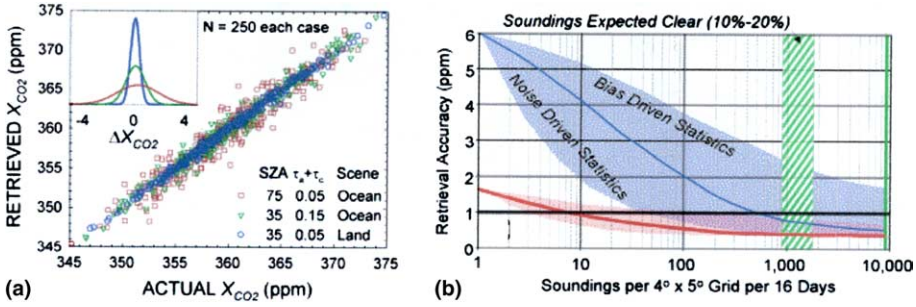

Fig. 4. (a) Retrievals of X_{CO_2} from individual simulated nadir soundings at solar zenith angles $\theta_0 = 35°$ and 75°. The model atmospheres include sub-visual cirrus clouds ($0.02 < \tau_c < 0.05$) and aerosols ($0.05 < \tau_a < 0.15$) over an ocean ($a \sim 0.05$) and desert ($a \sim 0.2$) surfaces. Inset: X_{CO_2} error distribution for each case, (b) Predicted accuracy of X_{CO_2} retrievals increases with the number of soundings. Cases with (red) and without (blue) the 2.06-μm CO_2 channel are shown for $\theta_0 = 37.5°$, albedo = 0.05, and aerosol optical depth, $\tau\{0.76\ \mu m\} = 0.15$. Results from sensitivity tests (solid lines) are shown with shaded envelopes indicating the range expected for error.

The OCO validation strategy will use ground-based solar-viewing Fourier Transform Infrared (FTIR) Spectrometers to tie the space-borne measurements of X_{CO_2} to in situ measurements. Solar-viewing FTIRs are well suited for the validation of OCO data because they measure the same quantity (the column-averaged mole fraction) and use the same O_2 and CO_2 absorption bands (Wallace and Livingston, 1990; Notholt et al., 1995; Yang et al., 2002). Because observations of direct sunlight are relatively insensitive to scattering by clouds and aerosols, comparisons between X_{CO_2} estimates from the satellite and ground-based FTIRs will permit independent assessment of systematic errors in the space-based retrievals due to clouds and aerosols.

OCO will deploy three dedicated FTIRs optimized for O_2 and CO_2 measurements at sites where in situ CO_2 observations are routinely performed. These systems will be similar to the one currently being installed at the WLEF tall tower site at Park Falls, Wisconsin (45.9°N, 90.3°W). Other candidate sites include the Atmospheric Radiation Monitoring (ARM) sites at Barrow, Alaska (71.3°N, 156.8°W) and Lamont, Oklahoma (36.6°N, 97.5°W), the Large-scale Biosphere-Atmosphere experiment (LBA) tower site at Floresta Nacional do Tapajos, Brazil (3.4°S, 54.9°W, and Cape Grim Baseline Air Pollution Station, Tasmania, Australia (40.4°S 144.4°E).

The OCO Project also plans to upgrade up to four existing FTIR spectrometers deployed by the Network for Detection of Stratospheric Change (NDSC). The NDSC FTIRs will be upgraded with detectors and beam splitters so that they measure X_{CO_2} in the OCO spectral regions. The preferred NDSC stations will: (1) be representative of the larger surrounding region (i.e. small gradients in X_{CO_2}, surface albedo, and topography) to facilitate comparisons with OCO, (2) have co-located in situ CO_2 observations, and (3) have an FTIR instrument that can be dedicated for X_{CO_2} observations. There are over 20 candidate sites including Ny Alesund (Spitsbergen), Fairbanks (Alaska), Kiruna, (Sweden) Wollongong (Australia), Arrival Heights (Antarctica), and Lauder, (New Zealand).

Ongoing aircraft campaigns will be augmented to characterize the vertical CO_2 profile above the FTS sites. CO_2 profiles, acquired in a vertical spiral from the surface to the tropopause will be obtained during an OCO Target overpass. These profiles will also be used to test whether the OCO retrievals correctly represent the X_{CO_2} variability at spatial scales of 10s to 100s of km. Data from other satellite experiments (e.g. Aqua and Aura) will be used to place the OCO soundings in the correct chemical, spatial, and temporal context. Correlative observations will include aspects of the CO_2 behavior not observable by OCO (e.g. diurnal variations, vertical profiles), and related atmospheric variables (e.g. CO, CH_4, aerosol) that will facilitate the interpretation of the X_{CO_2} data.

2.8. Laboratory spectroscopy requirements

The absorption line intensities and air-broadened line widths for the CO_2 and O_2 vibration–rotation bands used by OCO must be determined with accuracies of 0.3% or better to minimize systematic errors in comparisons between remote observations and in situ data. Because these requirements cannot be met by existing spectral line databases, the OCO team will make focused laboratory measurements of the bands used to retrieve X_{CO_2} The major error sources limiting the accuracies of laboratory line parameter measurements are uncertainties in the chemical composition of the sample and in the gas sample pressures and temperatures (Birk et al., 1996), as well as inadequate representation of the molecular and instrumental line shapes. Measurement accuracies of 0.3% have been obtained for diatomic molecules, such as CO, where an RMS uncertainty of 0.25% was recently obtained for 41 transition intensities by accurately characterizing the molecular and instrumental line shapes and retrieving line parameters from all spectra simultaneously (Jacquemart et al., 2001; Benner et al., 1995).

To decrease the errors in O_2 and CO_2 line intensity and width measurements from ~2.0% to 0.3%, we must improve several aspects of the experimental procedure. The McMath-Pierce Fourier transform spectrometer (FTS) at the National Solar Observatory (Kitt Peak, Arizona) has been baselined for these measurements. This instrument's line shape function is well characterized and it has a demonstrated capability to collect high SNR (1000:1), high spectral resolution (0.011 cm^{-1}) data. It will be upgraded with a new multi-pass absorption cell whose gas sample temperature and pressure sensors are calibrated to ±0.05%. The isotopic abundances and impurities in the gas samples will be calibrated by mass spectrometry to ±0.05%. The effective temperature of the gas in the cell will be validated by retrieving the rotational temperature from the measured line intensities. This system will be used to acquire numerous spectra of pure CO_2 and CO_2-air mixtures at relevant atmospheric temperatures and pressures to demonstrate reproducibility and improve the measurement precision to ~0.2% (Devi et al., 1998).

2.9. Source–sink inversion models

The X_{CO_2} fields retrieved by OCO will be used as inputs to synthesis inversion and data assimilation models. Synthesis inversion models solve the continuity equation to quantify the exchange of CO_2 between the atmosphere and the surface using precomputed atmospheric transport fields (wind fields, boundary layer dynamics). Such inversion calculations require high measurement accuracy, since the retrieved fluxes are sensitive to small (<0.3%) spatial and temporal errors in the measured

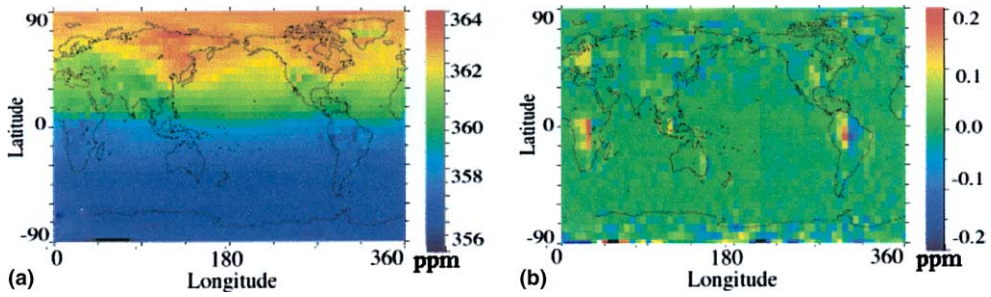

Fig. 5. (a) Calculated monthly mean, 24 h average X_{CO_2} (ppm) for May using the NCAR Match model driven by biospheric and fossil fuel sources of CO_2. (b) X_{CO_2} differences (ppm) between the monthly mean, 24-h average and the 1:15 PM value.

X_{CO_2} Assimilation methods optimally combine OCO observations with short-range forecasts. The high frequency, global analyses rely on the accuracy of the model and knowledge of spatial correlations in the data to provide information in regions with no observations. The products of these models will be a complete, dynamically self-consistent 4-D atmospheric CO_2 field that can be used for a number of purposes. To utilize OCO X_{CO_2} measurements, inversion models and data assimilation systems must correctly account for several types of sampling bias. These include the diurnal bias that results from the fixed 1:15 PM OCO orbit, as well as a clear-sky bias which results from the fact that OCO can acquire full-column measurements only on cloud-free days, when photosynthesis is expected to be stronger than on cloudy days.

2.10. Diurna bias

Measurements of the CO_2 volume-mixing ratio (vmr) show diurnal variations as large as 30% near the surface, but these variations decrease rapidly with altitude (15% at 22 m; Griffith et al., 2002). The net diurnal variation of the column-averaged CO_2 is estimated to be ~0.5% peak-to-peak over active forested regions, with the maximum occurring ~1 h after sunrise and the minimum ~1 h before sunset (Chou et al., 2002). On average, the X_{CO_2} measured by OCO at 1:15 PM will be ~0.1% below the 24 h mean. The X_{CO_2} measured by OCO may be biased to lower values over active forests than the surrounding areas (which have a smaller diurnal CO_2 variation), even if the actual diurnal mean CO_2 columns are identical over both regions. The CO_2 sink over active forests may be overestimated unless this bias is accounted for within inversion and data assimilation models.

We have used global Chemical Transport Models (CTMs) to assess the size of the diurnal bias. In these tests, we specified diurnal fluxes over continents from a 3-h ecosystem model that was tuned to meet a series of observational constraints. Fig. 5 shows results from the NCAR MATCH CTM driven by NCAR GCM. Panel 5a shows the calculated distribution of X_{CO_2} in May. Differences between the northern and southern hemispheres 6–8 ppm are apparent in the simulation. Panel 5b shows the difference between the monthly mean 24-h average value of X_{CO_2} and the monthly mean value of X_{CO_2} at 1:15 PM, the time of the OCO observation. This calculation suggests the diurnal bias of X_{CO_2} is small (differences <0.3 ppm), but potentially important when integrated over an annual cycle. Use of the ground-based observations will assure that the diurnal variation of CO_2 is considered properly in the determination of surface sources and sinks within assimilation models.

2.11. Clear-sky and seasonal biases

Another source of sampling bias arises from the fact that the space-borne measurements of X_{CO_2} will be obtained only in cloud-free conditions. In many ecosystems, photosynthesis will be stronger on sunny clays than on cloudy days, and so the value of X_{CO_2} measured by OCO may be biased slightly lower than average In tropical regions, highly productive forest ecosystems may have a greater degree of cloud cover as compared with savannas and deserts. Seasonal biases will be especially severe at high latitudes, which receive too little sunlight for solar X_{CO_2} measurements in winter. Full-column measurements are also precluded during persistently cloudy periods. Since X_{CO_2} is generally below average in the summer, models used to assimilate these observations must correctly represent the seasonal behavior to avoid sampling bias.

In situ measurements of CO_2 are critical for characterizing clear-sky or seasonal biases since they can be collected 24 h per day, 365 days per year, rain or shine. The in situ measurements of CO_2 obtained under this full range of observing conditions will be input to data assimilation models. By the time of the OCO launch, these models, will have the sophistication necessary to adjust key parameters (e.g., biospheric productivity, land and oceanic sinks) to match both the detailed day-to-day behavior of CO_2 recorded at the ground and the large-scale X_{CO_2}.

3. Instrumentation

The OCO instrument incorporates independent bore-sighted, long-slit, imaging grating spectrometers for the 1.61- and 2.06-μm CO_2 bands and the 0.76-μm O_2 A-band. These three spectrometers are integrated into a common structure to improve rigidity and thermal stability (Fig. 6). All three spectrometers use similar optical designs, consisting of an optimized 100 mm diameter, $f/2$ telescope that focuses light on a long, narrow slit that is aligned perpendicular to the orbit track. Behind the slit, the light is collimated, dispersed by a grating, and focused by a camera lens, forming a two-dimensional image of a spectrum on a 1024×1024 pixel focal plane array (FPA).

The spectrum is dispersed across the FPA in the direction orthogonal to the slit, and spatial information is recorded along the length of the slit. The slit length defines a 10-km wide cross-track swath at nadir from a 705-km orbit. This cross-track FOV is resolved by 160 pixels (16% of the array). These cross-track pixels are summed into 16-pixel bins to produce ten independent cross-track samples. The slit width defines a 0.13 km down-track instantaneous field of view (IFOV) at nadir from a 705 km orbit. By acquiring samples at 0.22-s intervals, the spacecraft motion provides down-track sampling of 1.5 km. Because the spectrometers have a fixed angular FOV, the size of the surface footprint increases when data are acquired in Target and Glint modes. For near-limb pointing, the cross-track IFOV expands to 4.4 km, but the down-track IFOV of the slit is still <1.5 km, yielding a footprint of $\sim$6.6 km^2. The optics, grating, and detector will be optimized to satisfy the spectral and spatial resolution and sampling requirements defined above. The read-out integrated circuits and signal processing electronics will be identical for the three FPAs, simplifying the design. The FPAs will be cooled to between 120 (2.06-μm channel) and 220 K (0.76-μm channel) by an active Sterling cycle cryocooler.

3.1. Instrument operational modes

There are three instrument modes: Operate, Standby and Off. The Operate mode includes Science and Calibration sub-modes. Data are collected in all operating modes. Identical operations are used for Nadir, Glint, and Target observations. There are four calibration modes, including dark (detector bias maps), lamp (detector gain maps), limb viewing (spectral line shape calibration) and solar viewing (absolute radiometric). Data are also collected in Standby mode, but they are not sent to the spacecraft's solid-state recorder.

4. Spacecraft and mission operations

4.1. Spacecraft

OCO will use a 3-axis stabilized spacecraft based on the Orbital LEOStar-2 bus (Fig. 3(a)). This bus was used previously for OrbView-4 (OV-4), Galaxy Explorer (GALEX), and Solar Radiation and Climate Explorer (SORCE). For OCO, the bus will be used to point the instrument to nadir, glint, specific ground targets, or the limb, or to orient the calibration target toward the sun. It will also be used to point the body-mounted X-band antenna at the ground station twice each day. The spacecraft includes a propulsion system to facilitate insertion into the EOS Afternoon Constellation, orbit maintenance, and a de-orbit maneuver at the end of the mission.

4.2. Mission operations overview

The OCO will be launched on a Taurus 2110 from the Western Test Range in mid-to-late 2007. It will fly at the front of the EOS Afternoon Constellation (A-Train), 15 min ahead of the Aqua spacecraft. The nominal mission duration is 2 years. The OCO instrument will operate continuously, but science data will be recorded only while over the sunlit hemisphere. About 5 min of calibration data will be taken during each orbit while the spacecraft is over the night side. Data will be transmitted to the ground at 150 megabits per second (Mbps) at X-band. The Universal Space Network (USN) will provide the X-Band downlink receiver. Fairbanks, Alaska has been designated as the primary downlink site. Four other high latitude USN stations are available

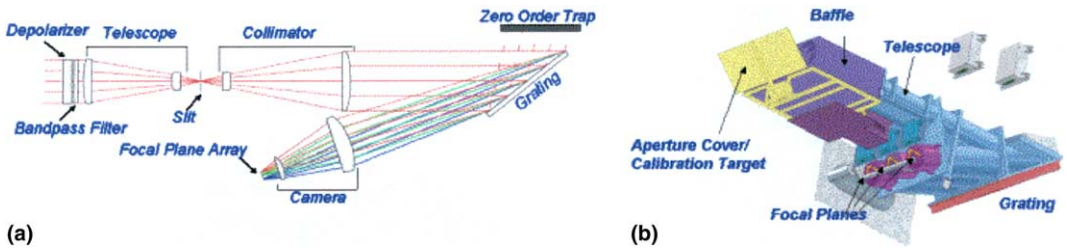

Fig. 6. (a) Major components of the optical system used by each of the three spectrometers. (b) Illustration showing physical layout of the three spectrometers. The aperture cover also serves as a calibration target.

for anomaly tracking and to provide resiliency in case of problems at the primary site.

Following launch, the 2-year mission begins with a 30-day checkout period followed by a 60-day period of initial science operations. For the remainder of the mission, the nominal plan is to switch from Nadir to Glint viewing modes once every ground repeat cycle, so that the entire Earth is covered by both modes about once each month. Target tracking campaigns (one target per orbit) occur at regular, but relatively infrequent intervals to support correlation with ground FTIR data and aircraft campaigns.

5. Conclusions

OCO will provide the first global, space-based observations of CO_2 with the spatial and temporal resolutions and accuracy needed to characterize sources and sinks of this important greenhouse gas. These space-based measurements will provide the greatest benefit in regions that are poorly sampled by existing ground-based CO_2 monitoring networks, but their high spatial density may also contribute to carbon cycle process studies, like those being planned as part of the North American Carbon Program. This information will help to provide a scientific basis for future atmospheric CO_2 mitigation strategies.

Acknowledgements

Part of this work was performed for the Jet Propulsion Laboratory of the California Institute of Technology under contract to NASA. Significant contributions were made by Hamilton Sundstrand Corporation (a United Technologies Company) and Orbital Sciences Corporation.

References

Baldocchi, D., Falge, E., Gu, L.H., Olson, R., et al. FLUXNET: a new tool to study the temporal and spatial variability of ecosystem-scale carbon dioxide, water vapor, and energy flux densities. Bull. Am. Meteor. Soc. 82, 2415–2434, 2001.

Battle, M., Bender, M.L., Tans, P.P., et al. Global carbon sinks and their variability inferred from atmospheric O_2 and $\delta^{13}C$. Science 287, 2467, 2000.

Benner, C.D., Rinsland, C.P., Devi, V.M., Smith, M.A.H. A multispectrum nonlinear least-squares fitting technique. J. Quant. Spectrosc. Radiat. Transfer 53, 705, 1995.

Birk, M., Hausamann, D., Wagner, G., Johns, J.W. Determination of line strengths by Fourier-transform spectroscopy. Appl. Opt. 35, 2971, 1996.

Bousquet, P., Peylin, P., Ciais, P., Le Quéré, C., et al. Regional changes in carbon dioxide fluxes of land and oceans since 1980. Science 290, 1342, 2000.

Chou, W.W., Wofsy, S.C., Harriss, R.C., Lin, J.C., et al. Net fluxes of CO_2 in Amazonia derived from aircraft observations. J. Geophys. Res. 107, 4614, 2002, 10.1029/2001JD001295.

Ciais, P., Tans, P.P., Trolier, M., et al. A large northern-hemisphere terrestrial CO_2 sink indicated by the $^{13}C/^{12}C$ ratio of atmospheric CO_2. Science, 269,1098, 1995.

Cicerone, R.J., Barren, E.J., Dickinson, R.E., Fung, I.Y., et al. Climate Change Science: An Analysis of Some Key Questions. National Research Council, Washington, DC, 2001.

Conway, T.J., Tans, P.P., Waterman, L.S., Thoning, K.W. Evidence for interannual variability of the carbon cycle from the National Oceanic and Atmospheric Administration Climate Monitoring and Diagnostics Laboratory global air sampling network. J. Geophys. Res. Atmos. 99, 22831, 1994.

Conway, T.J., Tans, P.P. Development of the CO_2 latitude gradient in recent decades. Glob. Biogeochem. Cycle 13, 821, 1999.

Cox, P.M., Berts, R.A., Jones, C.D., et al. Acceleration of global warming due to carbon-cycle feedbacks in a coupled climate model. Nature 408, 184, 2000.

Crisp, D. Absorption of sunlight by water vapor in cloudy conditions: a partial explanation for the cloud absorption anomaly. Geophys. Res. Lett. 24, 571, 1997.

Denning, A.S., Fung, I.Y., Randall, D. Latitudinal gradient of atmospheric CO_2 due to seasonal exchange with land biota. Nature 376, 240, 1995.

Devi, V.M., Benner, D.C., Rinsland, C.P., Smith, M.A.H. Absolute rovibrational intensities on $^{12}C^{16}O$ absorption bands in the 3090–3850 cm^{-1} spectral region. J. Quant. Spectrosc. Radiat. Transfer 60, 741, 1998.

Enting, I.G. Inverse problems in atmospheric constituent studies. 3. Estimating errors in surface sources. Inverse Probl. 9, 649, 1993.

Etheridge, D.M., Steele, L.P., Langenfelds, R.L., et al. Natural and anthropogenic changes in atmospheric CO_2 over the last 1000 years from air in Antarctic ice and firn. J. Geophys. Res. 101, 4115–4128, 1996.

Fan, S., Gloor, M., Mahlman, J., et al. A large terrestrial carbon sink in North America implied by atmospheric and oceanic carbon dioxide data and models. Science 282, 442, 1998.

Friedlingstein, P., Bopp, L., Ciais, P., Dufresne, J.L., et al. Positive feedback between future climate change and the carbon cycle. Geophys. Res. Lett. 28, 1543, 2001.

Frolking, S., Goulden, M.L., Wofsy, S.C., et al. Modeling temporal variability in the carbon balance of a spruce/moss boreal forest. Global Change Biol. 2, 343, 1996.

Gloor, M., Fan, S.M., Pacala, S., Sarmiento, J. Optimal sampling of the atmosphere for purpose of inverse modeling: a model study. Global Biogeochem. Cycle 14, 407–428, 2000.

Griffith, D.W.T., Jamie, I., Leuning, R., Denmead, T. Surface fluxes of CO_2, CH_4, and N_2O at OASIS'95 using tower-based FTIR techniques. Atmos. Environ. 36, 1833–1842, 2002.

Heidinger, A.K., Stephens, G.L. Molecular line absorption in a scattering atmosphere. Part II: application to remote sensing in the O_2 A-band. J. Atmos. Sci. 57, 1615, 2000.

Houghton, R.A. Interannual variability in the global carbon cycle. J. Geophys. Res. Atmos. 105, 20121, 2000.

Houghton, J.T., MeiraFilho, L.G., Callander, B.A., et al. Climate Change 2001: The Scientific Basis. Cambridge University Press, Cambridge, UK, 2001, 944pp.

Jacquemart, D., Mandin, J.Y., Dana, V., et al. A multispectrum fitting procedure to describe molecular line parameters: application to the 3-0 band of $^{12}C^{16}O$. Eur. Phys. J. D 14, 55, 2001.

Keeling, R.F., Shertz, S.R. Seasonal and interannual variations in atmospheric oxygen and implications for the global carbon cycle. Nature 358, 723, 1992.

Keeling, C.D., Whorf, T.P., Wahlen, M., Vanderplicht, J. Interannual extremes in the rate of rise of atmospheric carbon-dioxide since 1980. Nature 375, 666, 1995.

Kuang, Z., Margolis, J.S., Toon, G.C., et al. Spaceborne measurements of atmospheric CO_2 by high resolution NIR spectroscopy: an introductory study. Geophys. Res. Lett. 29, 2002, 1029/2001GL014298.

Langenfelds, R.L., Francey, R.J., Pak, B.C., Steele, L.P., et al. Interannual growth rate variations of atmospheric CO_2 and its isotope $\delta^{13}C$, H_2, CH_4 and CO between 1992 and 1999 linked to biomass burning. Global Biogeochem. Cycle 16, 1048, 2002.

Lee, K., Wanninkhof, R., Takahashi, T., et al. Low interannual variability in recent oceanic uptake of atmospheric carbon dioxide. Nature 396, 155, 1998.

Le Quéré, C., Orr, J.C., Monfray, P., et al. Interannual variability of the oceanic sink of CO_2 from 1979 through 1997. Global Biogeochem. Cycle 14, 1247, 2000.

Morimoto, S., Nakazawa, T., Higuchi, K., Aoki, S. Latitudinal distribution of atmospheric CO_2 sources and sinks inferred by $\delta^{13}C$ measurements from 1985 to 1991. J. Geophys. Res. Atmos. 105, 24315, 2000.

Notholt, J., Meier, A., Peil, S. Total column densities of tropospheric and stratospheric trace gases in the undisturbed Arctic; summer atmosphere. J. Atmos. Chem. 20, 311, 1995.

O'Brien, D.M., Mitchell, R.M. Error-estimates for retrieval of cloud-top pressure using absorption in the A-band of oxygen. J. Appl. Meteorol. 31, 1179, 1992.

Pacala, S.W., Hurtt, G.C., Baker, D., Peylin, P., et al. Consistent land- and atmosphere-based US carbon sink estimates. Science 292, 2316, 2001.

Randerson, J.T., Thompson, M.V., Conway, T.J., et al. The contribution of terrestrial sources and sinks to trends in the seasonal cycle of atmospheric carbon dioxide. Global Biogeochem. Cycle 11, 535, 1997.

Randerson, J.T., Field, C.B., Fung, I.Y., Tans, P.P. Increases in early season ecosystem uptake explain recent changes in the seasonal cycle of atmospheric CO_2 at high northern latitudes. Geophys. Res. Lett. 26, 2765, 1999.

Rayner, P.J., O'Brien, D.M. The utility of remotely sensed CO_2 concentration data in surface source inversions the seasonal cycle of atmospheric CO_2 at high northern latitudes. Geophys. Res. Lett. 28, 175, 2001.

Rayner, P.J., Law, R.M., O'Brien, D.M., Butler, T.M., Dilley, M. Global observations of the carbon budget: III. Initial assessment of the impact of satellite orbit, scan geometry and cloud on measuring CO_2 from space. J. Geophys Res. 107, Article 4557, 10.1029/2001JD000618, 2002.

Rodgers, C.D. Retrieval of atmospheric temperature and composition from remote sensing measurements of thermal radiation. Rev. Geophys. Space Phys. 14, 609, 1976.

Rodgers, C.D. Inverse Methods for Atmospheric Sounding: Theory and Practice. World Scientific Publishing Co. Pte. Ltd, Singapore, 256pp., 2000.

Schnell, R.C., King, D.B., Rosson, R.M. Climate Modeling and Diagnostics Laboratory Summary Report No. 25 (1998–1999). Report No. 25, 2001 and GLOBALVIEW-CO_2: Cooperative Atmospheric Integration Project-Carbon Dioxide, NOAA CMDL, Boulder, CO, 2001.

Tans, P.P., Conway, T.J., Nakazawa, T. Latitudinal distribution of the sources and sinks of atmospheric carbon dioxide derived from surface observations and an atmospheric transport model. J. Geophys. Res. 94, 5151, 1989.

Wallace, L., Livingston, W. Spectroscopic observations of atmospheric trace gases over Kitt Peak. 1. Carbon dioxide and methane from 1979 to 1985. J. Geophys. Res. Atmos. 95, 9823, 1990.

Yang, Z., Toon, G.C., Margolis, J.S., Wennberg, P.O. Atmospheric CO_2 retrieved from ground-based near IR solar spectra. Geophys. Res. Lett., 29, 2002, 10.1029/2001GL014537.